Effects of Thallium fluoride substitution on the flux pinning energies of $(Cu_{0.5}, Tl_{0.5})Ba_2Ca_2Cu_3O_{10-\delta}$ superconductors

M. S. Hassan[1] · A. Khalaf[2] · A. Kamar[3] · R. Awad[1,3] · M. Matar[1]

Abstract

In the present work, the magnetoresistance behavior of $(TlF)_x$-substituted $(Cu_{0.5},Tl_{0.5})Ba_2Ca_2Cu_3O_{10-\delta}$ superconducting samples, with $x = 0.0, 0.1, 0.2, 0.3$ and 0.4, was investigated. According to the thermally activated flux creep (TAFC) model, the flux pinning energies $U(H, T)$ were calculated from the resistivity temperature (ρ–T) curves at applied DC magnetic fields ranging from 0.29 to 4.44 kOe. The results indicated that flux pinning energy was increased with increasing the F-substituting up to $x = 0.1$ and then decreased with increasing the applied field up to 4.44 kOe. Moreover, significant resistive broadening (ΔT) was observed with increasing the values of the applied magnetic fields. Furthermore, the $(TlF)_x$ substitution, boosting the transport critical current density $J_c(0)$ and irreversibility magnetic field $H_{irr}(0)$ up to $x = 0.1$ and then decreasing for $x > 0.1$ at various applied magnetic fields, demonstrates strong flux pinning for $x = 0.1$.

Keywords (Cu, Tl)-1223 · Fluorine · Flux pinning · Magnetoresistance · Irreversibility field

1 Introduction

In high-temperature superconductors (HTSCs) such as (Cu, Tl)-1223, the vortex motion in the external magnetic fields is considered a crucial issue [1]. This vortex motion has the potential to rapidly destroy superconductivity [2]. The thermal fluctuations of the thermally activated flux flow (TAFF) alter vortex motion in the mixed state, causing a tail effect on the resistivity transition in the lower temperature region [3]. Although the pinning force is greater than the Lorentz force, which is created by the applied current on the flux bundle and results in energy dissipation, the vortex motion can still be produced via TAFF and flux creep [4]. Since the Ginzburg number, G, ($\sim 10^{-2}$–10^{-1}) of TAFF is of a high magnitude, it plays a highly useful role in ceramic superconductors. As a result, substantial thermal fluctuations in high-temperature superconductors (HTSCs), vortex phases, and dynamics vary [5, 6]. The

two distinct vortex phases, such as the liquid and glass phases, respectively, determine the normal and superconducting states [7]. Most of the dynamical complexity of the vortices is due to the battle between thermal fluctuations, arbitrary pinning, and the interaction of vortices [8]. At melting temperature, T_m, the Abrikosov vortex lattice is a first-order phase transition from a vortex liquid is specified in a pure phase [9–11]. Defects and disorders cause the vortex lattice to transition into the vortex glass phase, where the order of the phase transition from vortex liquid to vortex glass is regarded as second order [12, 13]. At the vortex glass phase transition temperature, T_g, numerous forms of vortex glass phases may exist depending on the nature and capabilities of the disorders [14]. In addition, a separate slushy vortex phase exists in systems with intermediate disorders in the temperature range of $T_m < T < T_g$. [15]. In pure phases, the slushy vortex phase transition can be conceived of as the remnant of a disordered first-order vortex lattice transition [8, 15]. The foregoing discussion has shown that flux pinning has a significant impact on superconductor transport parameters and that the vortex formation in HTSCs having poor pining flux capability is of fundamental relevance [16]. As a result, in addition to naturally occurring disorders, establishing artificial ones in the HTSCs lattices is an efficient way to prevent the motion of vortices and enhance the pinning flux and transport parameters of superconductors [16–18].

✉ M. S. Hassan
  mohammedscience2013@alexu.edu.eg

[1] Physics Department, Faculty of Science, Alexandria University, Alexandria, Egypt

[2] Physics Department, Faculty of Science, Damanhour University, Damanhour, Egypt

[3] Department of Physics, Faculty of Science, Beirut Arab University, Beirut, Lebanon

Most of the studies [19–21] concentrated on the effect of an applied external magnetic field on the resistive transition to better comprehend the mechanism of flux pinning and flux mobility. As a result, the thermally activated flux creep (TAFC) can adequately represent the data for the resistivity region approaching the zero-resistivity temperature T_{co} ($\rho = 0$) [22–24]. According to the TAFC model, in the presence of a magnetic field, the resistivity transition in HTSCs broadens and obeys the Arrhenius relation [25]:

$$\rho(H, T) = \rho_o \exp\left(-\frac{U(H, T)}{k_B T}\right), \tag{1}$$

where $U(H, T)$ is the pinning energy that depends on both temperature and magnetic field.

A power-law can be used to estimate the magnetic field dependence of flux pinning energy [26]:

$$U(H) \sim H^{-\beta}. \tag{2}$$

where β is a constant that depends on the magnetic field's orientation concerning the basal plane and the variety of applied magnetic fields.

In addition, the magnetic field dependence on transition width $\Delta T = (T_c - T_o)$ obeys a power-law [27]:

$$\Delta T \sim H^{(-n)} \sim H^{-\frac{\beta}{q}} \tag{3}$$

According to Ambegaokar–Halperin (AH) theory, the following relationship represents the magnetic field and temperature dependence of U [28]:

$$\frac{\rho}{\rho_n} = \left[I_o\left\{\frac{\gamma(H, T)}{2}\right\}\right]^{-2} \tag{4}$$

where I_o is the modified Bessel function, ρ_n is the resistivity in the normal state and γ is the Josephson coupling energy E_J to thermal energy ratio.

The Josephson coupling energy may be thought of as pinning energy, according to Tinkham's concepts [29, 30]:

$$\gamma(H, T) = \frac{E_J}{k_B T} = \frac{U(H, T)}{k_B T} \tag{5}$$

Finally, from the TAFC model and AH theory, $U(H, T)$ can be represented in the form [31]:

$$U(H, T) \sim \Delta T B^{(-\eta)}, \eta = \beta + n. \tag{6}$$

The distinction of thermal and magnetic field effects in the normalized barrier height can be rewritten from the physical image in AH theory as follows [32]:

$$\gamma(H, T) = C(H)(1 - t)^q, \tag{7}$$

where $t = T/T_c$ denotes the reduced temperature and $q = \beta/n$. The magnetic field-dependent parameter, $C(H)$, is used to

calculate the critical current density at 0 K and is given as [33]

$$J_c(0) = C(H) e K_B T_C / \hbar d^2. \tag{8}$$

where d is the average grain size determined using scanning electron microscope images.

In the present work, the effects of F-substituted (Cu, Tl)-1223 samples on the flux pinning energy using the thermally activated flux creep (TAFC) model under different applied fields in the range of 0.29–4.44 kOe were studied. Moreover, the dependence of the critical currents on external magnetic fields and the irreversibility fields was investigated.

2 Materials and methods

A single-step solid-state reaction method was successfully used to prepare superconducting samples of $(Cu_{0.5}, Tl_{0.5})Ba_2Ca_2Cu_3 O_{10-\delta}$ that were substituted with varying amounts of $(TlF)_x$ at the Tl site with $x = 0.0, 0.1, 0.2, 0.3,$ and 0.4. The nominal composition of the starting reagents is $(Cu0.5[Tl_{0.5-x}]_{Tl2O3}[Tl_x]_{TlF})Ba_2Ca_2Cu_3O_{10-\delta}F_x$, where the TlF is used as a source of fluorine to substitute the F ion at the O site and is directly mixed with the other starting reagents from the beginning. The preparation and characterization of the samples have been described in detail elsewhere [34]. The temperature dependence of the resistivity under different magnetic fields ranging from 0.29 to 4.44 kOe at a constant deriving current of 1 mA was obtained by employing the four-probe method. With the aid of helium gas through a cryogenic diplex system, the refrigeration of the samples was done until the temperature reached its zero-resistivity temperature (T_o). The samples had dimensions of about $1.2 \times 0.4 \times 0.4$ cm^3 and the connection of the copper leads with the samples was made using conductive silver paste. The temperature of the sample was monitored by a Chromel versus Fe–Au thermocouple and stabilized with the aid of a temperature controller to within ± 0.1 K. The potential drop across the sample was measured using a Keithley 181 digital nano voltmeter. The voltage was determined by taking the average of the values measured with the normal and the reverse directions of the applied current to eliminate the thermoelectric voltages of the junction leads. The measurements were carried out in a magnetic field upon heating after zero-field cooling (ZFC). The generated magnetic field from a DC electromagnet is applied normally to the direction of the driving current.

3 Results and discussion

The room temperature XRD patterns of the prepared samples: $(Cu_{0.5}[Tl_{0.5-x}]_{Tl2O3}[Tl_x]_{TlF})Ba_2Ca_2Cu_3O_{10-\delta}F_x$, with $x = 0.0, 0.1, 0.2, 0.3$ and 0.4, are depicted in Fig. 1. The

diffraction peaks are mostly associated with the tetragonal structure of the (Cu, Tl)-1223 phase, which has the space group P4/mmm [35] with limited indexed low-intensity peaks suggesting the existence of both the (Cu, Tl)-1212 phase and $BaCuO_2$. Kamar et al. [34] previously reported on the features and examinations of these samples, and the results are compiled in Table 1.

The superconducting properties of the (Cu, Tl)-1223 system are dependent on the hole concentration or the number of holes per Cu-atom [36, 37]. A parabolic relationship [38] holds between the superconducting transition temperature and the hole concentration as indicated in the following equation:

$$T_c/T_c^{max} = 1 - 82.6(P - 0.16)^2 \qquad (9)$$

where P represents hole concentration and T_c^{max} is taken as 132 K for the (Cu, Tl)-1223 system [39]. The superconducting transition temperature, T_c, which corresponds to the curve's maximum, can be determined using Gaussian fitting of the temperature dependence of the $d\rho/dT$ curves as pictured in Fig. 2. The T_c value of the pure sample was around 119.5 K. It rises by 4.82% to reach its optimum value at 124.5 K for $x = 0.1$, and then it declines by 6.41% to 117 K for $x = 0.4$. The preliminary rise in Tc may have been caused by many reasons, including the boosting of the forming of the main ($Cu_{0.5}Tl_{0.5}$)-1223 superconductor phase, as shown by XRD measurements and the creation of cooper pairs during the transition from the normal to the superconducting states by the partial replacement of oxygen with fluorine [40]. Moreover, Tl-based oxides are over-doped with a value of hole concentration in the Cu–O planes greater than the optimum one related to the optimum T_c. As T_c was found to increase by removing oxygen from the structure by F-substitution resulted in reducing hole concentration and optimizing superconducting features at an optimum concentration of $x = 0.1$. These findings are consistent with XRD and RBS analysis. On the other hand, T_c suppressions for $x > 0.1$ might well be associated with a boost in the volume fraction of impurity phases, as assisted by XRD analysis. It could also
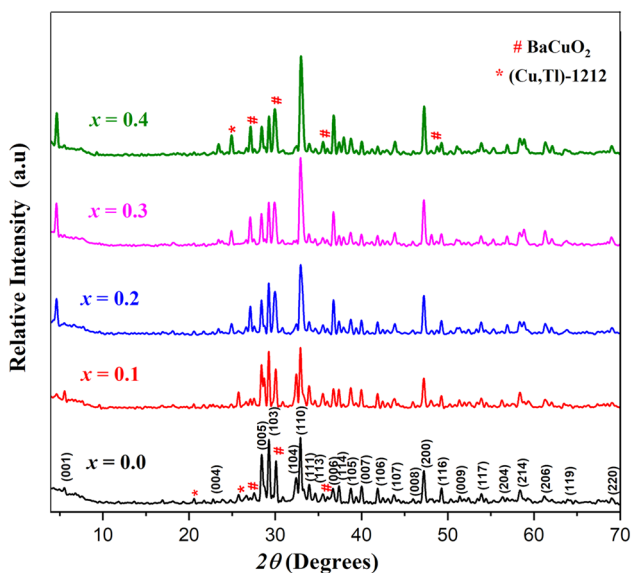

Fig. 1 XRD patterns of $(TlF)_x$ doped (Cu, Tl)-1223 with $x = 0.0$, 0.1, 0.2, 0.3, and 0.4. The peaks indexed by (*) and (#) represent (Cu, Tl)-1212 and $BaCuO_2$
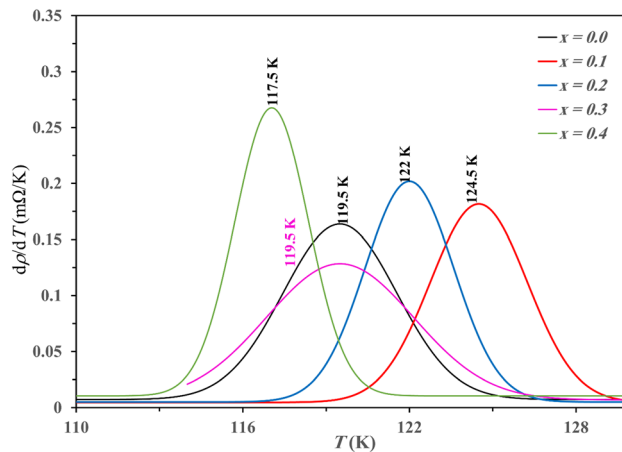

Fig. 2 Variation of resistivity derivative concerning temperature for all samples

Table 1 The lattice parameters (a and c), the O and F elemental content [34], hole concentration (P), thermoelectric power (S), and fitting parameters for magnetoresistance (β, n, η, and q) of the ($Cu_{0.5}$, $Tl_{0.5}$)-1223 phase with $(TlF)_x$ substitution, $0.0 \leq x \leq 0.4$.

x	Lattice parameter (Å)		Elemental content		P	S (µV/K)	β	n	η	q
	a	c	O	F						
0.0	3.858 (4)	15.852 (3)	9.800	0.000	0.194	3.35	0.229	0.250	0.479	0.916
0.1	3.843 (4)	15.874 (4)	9.706	0.095	0.186	7.63	0.281	0.319	0.592	0.900
0.2	3.833 (3)	15.882 (6)	9.454	0.261	0.190	5.34	0.210	0.244	0.454	0.862
0.3	3.833 (7)	15.911 (9)	9.423	0.284	0.194	2.98	0.197	0.294	0.491	0.670
0.4	3.827 (1)	15.920 (3)	N/D	N/D	0.196	1.92	0.160	0.268	0.428	0.597

be due to the trapping of mobile holes and some mechanisms associated with oxygen vacancy disorder. [41] The estimated values of hole concentration are represented in Table 1. It is obvious that P values decrease with increasing F-substituting up to $x = 0.1$ and reach their optimum value of T_c at 124.5 K. For more additive values of F-substituting, they decrease and reach the minimum values of T_c at 117.5 K. The charge carrier transport mechanism in high-T_c superconductors determines thermoelectric power, S, and is given by [42]

$$S = \frac{k_B}{e}\left[\ln(\frac{1-p}{2P}) - \ln 2\right] \tag{10}$$

where k_B is the Boltzmann constant and e is the electron charge. As seen in Table 1, all the thermoelectric power values are positive, indicating that hole conduction is the primary mechanism. Thermoelectric power is generally understood to be extremely sensitive to oxygen doping, which is closely connected to T_c. The maximum value of thermoelectric power for $x = 0.1$ confirmed that the sample is ideally doped in the CuO_2 layer with 0.186 holes per Cu-atom.

F^- can be substituted into a structure in one of three ways [43]: (i) by directly replacing an O^{2-} ion with an F^- ion; (ii) by replacing one O^{2-} ion with one or more F ions; or (iii) by adding F ions to the structure's interstitial spaces. The successful replacement of oxygen ions with fluorine ions has a few justifications. This is further discussed as follows: (i) According to the XRD analysis of Fig. 1, there is no appreciable impact on the samples' tetragonal structure and the locations of the diffraction peaks. Due to the similarities in the ionic radii of O^{2-} and F^- (140 and 136 pm, respectively), for VI coordination number) [44], it indicates that F ions can easily replace O_2. As evidenced further by the variation of the lattice parameters (a and c), whose values slightly drop and rise, respectively. Abu Hlaiwa et al. [24] and Anas et al. [45] came to similar findings when examining the impact of PbF_2 on the physical characteristics of the (Cu, Tl)-1223 and (Bi, Pb)-2223 superconducting phases, respectively. (ii) The charge balancing issues caused by the substitution of fluorine ions for oxygen ions should lead to a reduction in the carrier (holes) density in p-type superconductors [43]. This is supported by the positive values of the S and P as presented in Table 1, which demonstrate the strong link between the improvement in T_c values up to $x = 0.1$ with rising F-content and falling oxygen content. Saoudel et al. [46] reported a similar pattern of behavior when examining the impact of doping TlF_3 on the superconducting characteristics of (Bi, Pb)-2223 phase. (iii) As can be observed from Table 1, which summarizes the results of the PIGE and RBS methods used to calculate the fluorine content values. The values are nearly equal to those of x

and rise with increasing TlF substitution concentrations. It was expected that the oxygen content would decrease as fluorine ions replaced oxygen ions.

The magnetic field dependence of resistivity with respect to temperature of the $(Cu_{0.5}[Tl_{0.5-x}]_{Tl2O3}[Tl_x]_{TlF})$ $Ba_2Ca_2Cu_3O_{10-\delta}F_x$, with $0.0 \leq x \leq 0.4$, at different applied magnetic fields of 0.00, 0.29, 1.2, 2.34, 3.53, and 4.44 kOe is shown in Fig. 3 (a–e). There are two regions where the magnetic field can affect the resistivity curve. The first one occurs in the normal-state region ($T > T_c$), where normal-state resistivity changes vary very slightly when the applied magnetic field increases due to defects and inhomogeneities in the samples [47, 48]. The mixed state region that contains both the pairing transition and the tail parts is the second one. The pairing transition part, which is connected to the transition of isolated grains to the superconducting state, T_c^{onset}, may alter somewhat when magnetic fields are applied, indicating the significant intra-grain energy that restricts vortex motion [49]. On the other hand, the broadening tail part of resistivity is more sensitive to the applied magnetic field, even at low values, due to flux penetration into the inter-granular regions of the weak coupling between grains and shifts to lower temperatures as the applied magnetic field increases [50].

In addition, when the applied field increases, the T_{co} of F-substituted (Cu, Tl)-1223 samples decreases regularly toward lower temperatures, as seen in Fig. 3. By substituting with fluorine ions, the resistive tail decreases up to $x = 0.1$, then it increases up to $x = 0.4$. This increase could be due to the increased volume fraction of the samples in the mixed state. At lower temperatures, the pinning disorder and pinning interaction should dominate thermal effects at the vortex glass phase $T < T_g$, where T_g is the glass transition temperature that separates between the liquid vortex phase ($T > T_g$) and the glass vortex phase ($T < T_g$). The Vogel–Fulcher relation $(d ln\rho/dT)^{-1} \propto (T - T_g)$ [51] was used to calculate T_g. Figure 4 shows the variation of T_g versus the applied magnetic fields for F-substituted (Cu, Tl)-1223 samples. It follows that the values of the T_g decrease as the applied magnetic field increases. To further understand the effect of F-substitution, a further investigation was conducted into the flux pinning energy, transport critical current density, and irreversibility field of the samples [22].

The graphs of ln (ρ) vs $1/T$ for $(Cu_{0.5}[Tl_{0.5-x}]_{Tl2O3}[Tl_x]_{TlF})$ $Ba_2Ca_2Cu_3O_{10-\delta}F_x$, with $0.0 \leq x \leq 0.4$, are shown in Fig. 5 (a-e). The flux pinning energy, U, could be evaluated from the slope of linear data points in the tail part as a function of the applied magnetic fields as represented in Fig. 5. It is noted that, as the applied magnetic field was raised to $H = 1.2$ kOe, the U values for all F-substituted samples rapidly declined, owing to weak links in the inter-granular spaces [52]. Following that, by raising the applied field strength to $H = 4.44$ kOe, the drop in U decreased and essentially
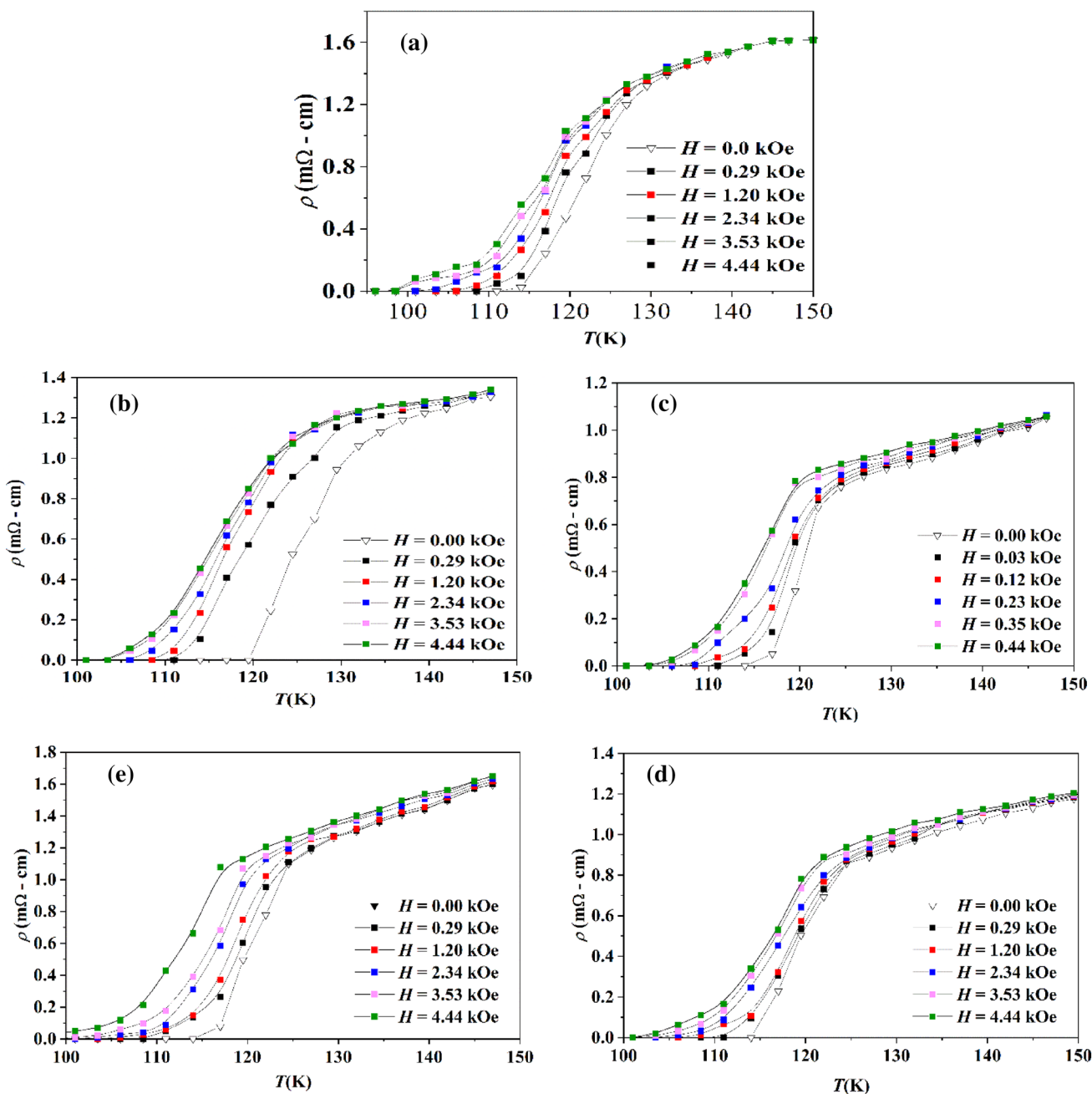
Fig. 3 The temperature dependence of resistivity of (Cu$_{0.5}$[Tl$_{0.5-x}$]$_{Tl2O3}$[Tl$_x$]$_{TlF}$)Ba$_2$Ca$_2$Cu$_3$O$_{10-\delta}$F$_x$, samples with (**a**) $x=0.0$, (**b**) $x=0.1$, (**c**) $x=0.2$, (**d**) $x=0.3$ and (**e**) $x=0.4$ at different magnetic fields

plateaued. This could be owing to a larger external magnetic field causing an increase in the population of vortices [53]. Furthermore, as F-substitution increases, the flux pinning energies of U increase until they reach an optimum level of $x=0.1$, confirming T_c behavior. An increase in F-content up to $x=0.1$ produces an increase in the number of pinning centers, supporting an improvement in their flux pinning character, which may improve the energy barriers needed for flux pinning. Similar results were reported by Shakil et al.

[50]. U decreases as $x > 0.1$, and the weak links increase, causing the vortices to creep more easily [54].

According to Eq. (2) and the data extracted from Fig. 6, for each sample, the β value is obtained and listed in Table 1. The value of β varies between 0.16 and 0.28. This is similar to the results (0.28–0.33) reported for Zn and Ni-doped Tl-1223 [55], but less than the results (0.39–0.69) obtained for Sc-doped Tl-1223 [56]. However, there are no expected values of β since they are extremely sensitive
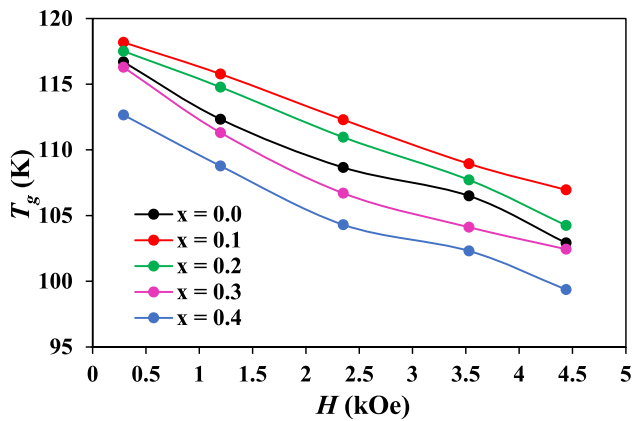
Fig. 4 The variation of T_g with the applied field magnetic field for F-doped samples

to numerous factors affecting the U and crystal structure features, such as weak link quality, oxygen content, and atom position.

The variation of ΔT versus H for F-substituting samples is illustrated in Fig. 7, according to Eq. (3). The high number of randomly oriented grains that freeze and cluster in random places during the cooling process increases ΔT for all samples as the applied magnetic field increases. As a result, the samples contain more resistive regions, resulting in weaker vortex pinning as the superconducting current path is shortened. Furthermore, a reduction in the microscopic inhomogeneous superconducting phase and/or an increase in inter-grain connection might be attributed to a decrease in ΔT with F-substituting up to $x = 0.1$.

The Ambegaokar and Halperin (AH) theory [57] is used to analyze the effect of an applied magnetic field on the motion of a flux line. The AH theory describes how the phase of the order parameter is affected by thermal fluctuations throughout a current-driven Josephson junction [33]. Table 1, which also demonstrates the change of the estimated parameters β, n, η, and q versus (TlF)x-substituting, according to AH theory. It is found that n and q decrease until $x = 0.1$, after which they increase as x increases further. This could be due to the F-substituted (Cu, Tl)-1223 phase formation being suppressed at $x > 0.1$. Equation (8) can be used to calculate $J_c(0)$ using the magnetic field-dependent $C(H)$ parameter. The variation of $J_c(0)$ vs H for $(Cu_{0.5}[Tl_{0.5-x}]_{Tl2O3}[Tl_x]_{TlF})Ba_2Ca_2Cu_3O_{10-\delta}F_x$, samples are depicted in Fig. 8. The single-junction sensitivity to the applied magnetic field between superconducting grains is demonstrated by the drop in $J_c(0)$ in grain borders when the field is increased. The $J_c(0)$ is improved by increasing

F-substituting up to $x = 0.1$. This improvement might be explained by the impact of F-substituting in enhancing flux pinning, acting as pinning centers or establishing locally weak superconducting zones. In addition, when $x > 0.1$, the decrease in $J_c(0)$ could be owing to an increase in grain boundary resistance or non-superconducting impurities.

The irreversibility line of high-T_c superconductors, which separates the vortex glassy and vortex liquid states on the H–T phase diagram, is the most prominent curve [58]. This line is formed by the irreversibility fields' temperature dependency, and the flux lines are driven to move above it by the flowing current. It indicates that energy has been dissipated and that the supercurrent has vanished. In this aspect, the irreversibility field of high-T_c superconductors is comparable to the upper critical field of conventional superconductors. As illustrated in Fig. 9, the irreversibility field $H_{irr}(T)$ was calculated by calculating 10% of normal resistivity from magnetoresistance measurements. The stabilization of flux lines into (Cu, Tl)-1223 samples following F-substituting is confirmed by a larger H_{irr} value, which correlates to better flux pinning.

The temperature dependency of the irreversibility field is given as [59, 60]

$$H_{irr}(T) = H_{irr}(0)(1 - T/T_{c0})^m \tag{11}$$

where $H_{irr}(0)$ is the irreversibility field at 0 K, T_{c0} is the zero-resistivity temperature at zero magnetic fields and the exponent m (theoretically equals 3/2) can vary widely depending on the vortex properties.

Table 2 shows the fitted parameters n and $H_{irr}(0)$ according to Eq. (9). It is clear, for all samples, that the H_{irr} sample is given by nearly exponent $m \sim 1.5$, within the range of measurement temperatures. This suggests that H_{irr} is affected by the flux creep phenomenon.

4 Conclusion

The magnetoresistance of the F-substituted (Cu, Tl)-1223 phase was investigated, and the results were explained within the AH model. The flux pinning strength obtained from Arrhenius plots was improved by increasing F-substituting up to $x = 0.1$, which decreased. In addition, it was decreased by applying a magnetic field. The increasing transition width region was due to the dissipation of energy caused by the motion of vortices because of the enhanced volume fraction of the sample in the mixed state. The calculated parameters like $J_c(0)$, and $H_{irr}(0)$ were also enhanced by F-substituting
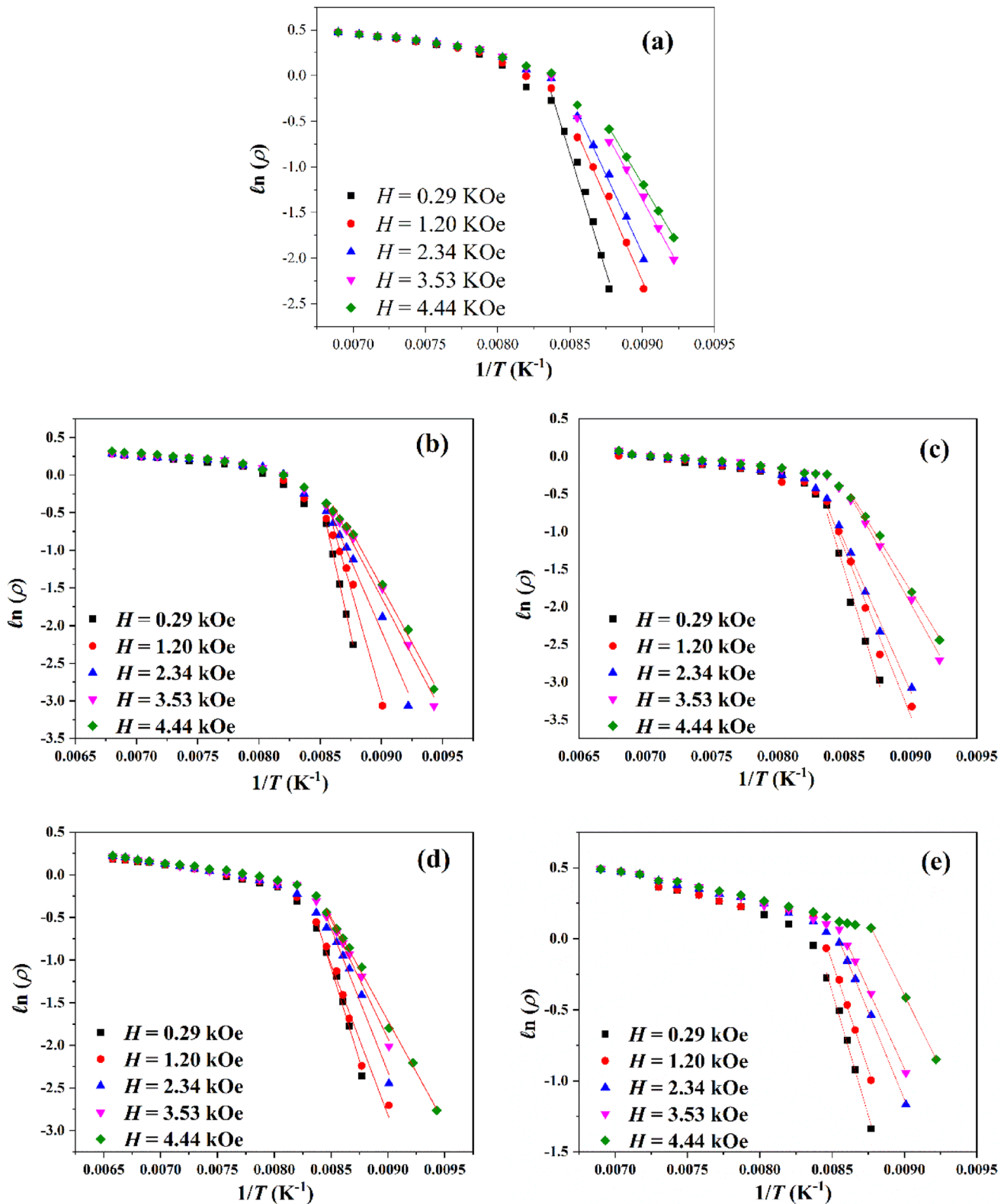
Fig. 5 ℓn(ρ) vs 1/T for (Cu$_{0.5}$[Tl$_{0.5-x}$]$_{Tl2O3}$[Tl$_x$]$_{TlF}$)Ba$_2$Ca$_2$Cu$_3$O$_{10-\delta}$F$_x$, with (**a**) $x=0.0$, (**b**) $x=0.1$, (**c**) $x=0.2$, (**d**) $x=0.3$, and (**e**) $x=0.4$ at different magnetic fields.
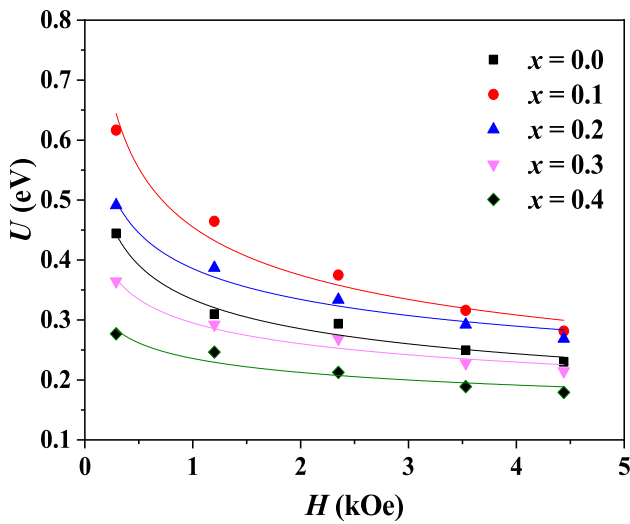
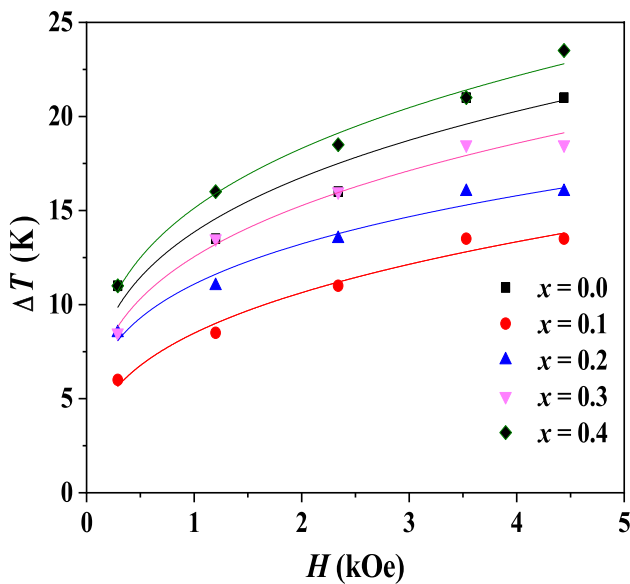**Fig. 6** The flux pinning energy $U(H)$ versus magnetic field for F-doped samples

Fig. 7 The transition width ΔT vs. applied magnetic field for all samples

Fig. 8 The critical current density $J_c(0)$ versus magnetic field for all samples
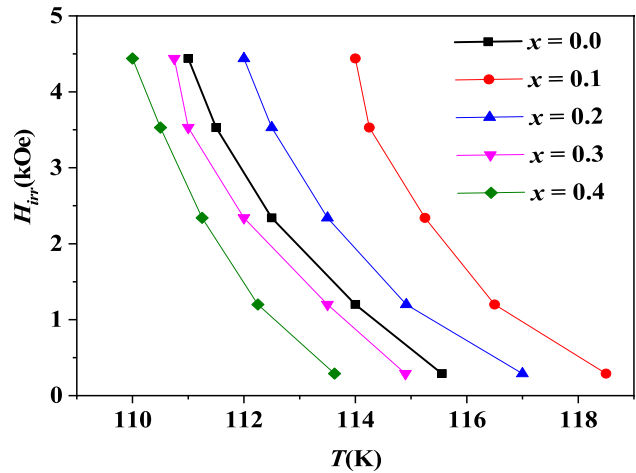
Fig. 9 The irreversibility field H_{irr} versus T for all samples

Table 2 Fitted parameters m and $H_{irr}(0)$ of all samples

x	m	$H_{irr}(0)$ (kOe)
0.0	1.50	421.09
0.1	1.54	437.13
0.2	1.46	426.17
0.3	1.48	418.26
0.4	1.41	415.34

up to $x = 0.1$, indicating that F-substituting can act as pinning centers or generate locally weak superconducting regions, which improved superconducting magnetic properties. The irreversibility line of H_{irr} was fitted with the power-law dependence $(1 - T/T_{co})^m$ with $m \sim 1.5$, confirming the flux creep is present in our samples.

Data Availability The data that support the findings of this study are available from the corresponding author upon reasonable request.

Declarations

Conflict of interest No potential conflict of interest was reported by the authors.

References

1. A. Labrag, M. Bghour, A. Abou El Hassan et al., Eur. Phys. J. Appl. Phys. **92**, 20601 (2020)
2. G. Hussain, A. Jabbar, I. Qasim et al., J. Appl. Phys. **116**, 103911 (2014)
3. W.J. Choi, Y.I. Seo, D. Ahmad et al., Results Phys. **19**, 103430 (2020)
4. R. Wördenweber, Phys Sci Rev. (2017). https://doi.org/10.1515/psr-2017-8000
5. Y. Jang Song, B. Kang, J.S. Rhee et al., EPL Europhys. Lett. **97**, 47003 (2012)
6. G.P. Mikitik, E.H. Brandt, Phys Rev B. (2001). https://doi.org/10.1103/PhysRevB.64.024505
7. R. Kumar, G.D. Varma, Phys. Scr. **95**, 45814 (2020)
8. X. Xing, X. Yi, M. Li et al., Supercond. Sci. Technol. **33**, 114005 (2020)
9. H. Safar, P.L. Gammel, D.A. Huse et al., Phys. Rev. Lett. **69**, 824 (1992)
10. W.K. Kwok, J. Fendrich, S. Fleshler et al., Phys. Rev. Lett. **72**, 1092 (1994)
11. U. Welp, J.A. Fendrich, W.K. Kwok et al., Phys. Rev. Lett. **76**, 4809 (1996)
12. D.S. Fisher, M.P.A. Fisher, D.A. Huse, Phys. Rev. B. **43**, 130 (1991)
13. R.H. Koch, V. Foglietti, W.J. Gallagher et al., Phys. Rev. Lett. **63**, 1511 (1989)
14. T. Nishizaki, T. Naito, N. Kobayashi, Phys. Rev. B. **58**, 11169 (1998)
15. T.K. Worthington, M.P.A. Fisher, D.A. Huse et al., Phys. Rev. B. **46**, 11854 (1992)
16. S. Arumugam, M. Krishnan, K. Ishigaki et al., Sci. Rep. **9**, 347 (2019)
17. J.J. Giapintzakis, W.C. Lee, J.P. Rice et al., Phys. Rev. B. **45**, 10677 (1992)
18. W.J. Choi, D. Ahmad, Y.I. Seo et al., Sci. Rep. **10**, 2017 (2020)
19. A. Jukna, I. Barboy, G.J. Jung, Appl. Phys. **99**, 113902 (2006)
20. M.H. Pu, Z.S. Cao, Q.Y. Wang et al., Supercond. Sci. Technol. **19**, 462 (2006)
21. A. Pandey, D. Bhattacharya, R.G. Sharma, Physica C. **340**, 211 (2000)
22. T.T.M. Palstra, B. Batlogg, L.F. Schneemeyer et al., Phys Rev Lett **61**, 1662 (1988)
23. R. Griessen, Phys. Rev. Lett. **64**, 1674 (1990)
24. B. Özkurt, B. Özçelik, J Low Temp Phys. (2009). https://doi.org/10.1007/s10909-009-9899-6
25. A. Abou-Aly, M. Mostafa, I. Ibrahim et al., Supercond. Sci. Technol. **15**, 938 (2002)
26. M. Me, Barakat Results Phy. **7**, 1181 (2017)
27. B. Özçelik, M. Gürsul, F. Karaçora Nane et al., Effect of Na-substitution on magnetoresistance and flux pinning energy of Bi-2212 ceramics prepared via hot-forging process. J Mater Sci Mater Electron. (2018). https://doi.org/10.1007/s10854-018-0041-x
28. V. Ambegaokar, B.I. Halperin, Voltage due to thermal noise in the dc Josephson effect. Phys Rev Lett. **22**, 1364 (1969)
29. M. Tinkham, Phys. Rev. Lett. **61**, 1658 (1988)
30. M. Tinkham, C.J. Lobb, Solid State Phys. (1989). https://doi.org/10.1016/S0081-1947(08)60080-6
31. H. Khosroabadi, V. Daadmehr, M. Akhavan, Phys C (2003). https://doi.org/10.1016/S0921-4534(02)01876-2
32. N.H. Mohammed, A.I. Abou-Aly, R. Awad et al., Supercond Sci Technol **19**(11), 1104 (2006)
33. H.S. Gamchi, G.J. Russel, K.N.R. Taylor, Phys Rev B **50**, 12950 (1994)
34. A. Kamar, A. Srour, W. Malaeb et al., Appl. Phys. A **127**(8), 579 (2021)
35. T. Hopfnger, O.O. Shcherban, P. Galez, R.E. Gladyshevkii, M. Lomello-Tafn, J.L. Jorda, M. Couach, J. Alloy. Compd. **333**, 237 (2002)
36. A. Srour, W. Malaeb, S. Marhaba et al., J Phys Conf. Series **869**(1), 012017 (2017)
37. N.M. Hamdan, M. Faiz, M.A. Salim, A. Hasan, Z. Hussain, AIP Conf. Proc. **10**(1063/1), 1757980 (2004)
38. S.B. Guner, Y. Zalaoglu, T. Turgay et al., J Alloys Comp. **772**, 388 (2019)
39. M. Mumtaz, Z. Iqbal, M.R. Hussain, A. Liaqat, M. Waqee-ur-Rehman, M. Saqib J Supercond Nov Magn **31**, 1315 (2018)
40. N.M. Hamdan, K.A. Ziq, A.S. Al-Harthi, Physica C **314**, 125 (1999)
41. M. Mumtaz, N.A. Khan, Supercond. Sci. Technol. **21**, 065015 (2008)
42. J.R. Cooper, B. Alavi, L.W. Zhow, W.P. Boyermann, G. Gruner, Phys. Rev. B **35**, 8794 (1987)
43. M.G. Francesconi, C. Greaves, Supercond. Sci. Technol. **10**, A29 (1997)
44. R.D. Shannon, Acta Crystallogr. A **32**, 751 (1976)
45. M. Anas, Chem. Phys. Lett. **742**, 137033 (2020)
46. A. Saoudel, A. Amira, N. Mahamdioua, Y. Boudjadja, A. Varilci, S.P. Altintas, C. Terzioglu, Improvement of superconducting properties of (Bi, Pb)-2223phase by TlF3 doping. Physica B. **501**, 61 (2016)
47. A. Aliabadi, Y.A. Farshchi, M. Akhavan, Phys C Superconduct Appl. (2009). https://doi.org/10.1016/j.physc.2009.09.003
48. C. HaiFeng, L. Jie, L. Shao et al., Sci China Phys Mech Astron **53**(7), 1180 (2010)
49. E. Gross, P. Chaudhari, D. Dimos, A. Gupta, G. Koren, Phys. Rev. Lett. **64**, 228 (1990)
50. A. Shakil, K. Nawazish, A. Khurram et al., J Supercond Nov Magn. **27**, 2787 (2014)
51. A. Takeuchi, A. Inoue, Mater. Trans. **43**(5), 1205 (2002)
52. M. Me, Barakat, K. Habanjar, J Advan Ceramic. (2017). https://doi.org/10.1007/s40145-017-0222-8
53. T.T.M. Palstra, B. Batlogg, R.B. van Dover et al., Phys. Rev. B **41**, 6621 (1990)

54. M.R. Mohammadizadeh, M. Akhavan, Supercond Sci Tech. **16**, 538 (2003)

55. M. Waqee-ur-Rehman, M. Mumtaz, M. Qasim et al., Solid State Comm. **228**, 32–35 (2016)

56. A.I. Abou-Aly, S.A. Mahmoud, R. Awad et al., J Supercond Nov Magn **23**, 1575 (2010)

57. V. Ambegaokar, B.I. Halperin, Phys. Rev. Lett. **22**, 1364 (1969)

58. J.R.L. de Almeida, D. Thouless, J. Phys. A **11**, 983 (1978)

59. K.A. Muller, M. Takashige, J.G. Bednorz, Phys. Rev. Lett. **58**, 1143 (1978)

60. W.M. Woch, R. Zalecki, A. Kołodziejczyk et al., Phys. C. **434**, 17 (2006)